ADVANCED MATERIALS
www.advmat.de

www.MaterialsViews.com

Spintronic Functionality of $BiFeO_3$ Domain Walls

Ji Hye Lee, Ignasi Fina,* Xavi Marti, Young Heon Kim, Dietrich Hesse, and Marin Alexe**

Before the dawn of multiferroics, ferroelectricity, and ferromagnetism had independently succeeded in the realms of fundamental research, sensing and memory technologies. Over a decade ago, the coupling of two ferroic properties in a single material revived as a promising direction. However, most of its realizations have remained limited to heterostructures merging the ferroelectric (FE) and ferromagnetic (FM) orders at their interfaces and/or interconnected via strain fields.[1] Here, it is proposed to make use of the FE domain walls (DWs) in the multiferroic material $BiFeO_3$ (BFO), which are also conducting and FM, and which are intrinsically two dimensional nano-objects of multiferroic type in a single material. It is also shown that one can modulate the electronic transport across the – FM and FE – domain walls in BFO via an external magnetic field, resembling the anisotropic magnetoresistance (AMR) in archetypical metallic ferromagnets. At the same time, BFO preserves two stable and switchable electric polarization states and one can manipulate the FE DWs, and thus magnetization, via an electric field.

Lord Kelvin initiated the field of spintronics in 1856 with the discovery of anisotropic magnetoresistance (AMR) in Ni and Fe.[2] Few decades later, Valasek published the seminal work on ferroelectricity of Rochelle salt in 1921.[3] Today, the scarcity of materials exploiting both spintronics and ferroelectricity has been standing for over a decade, since insulating ferroelectrics usually exclude any electronic transport and thus any sort of spin-dependent transport. Recently, the discovery of conductive domain walls in BFO,[4] and the corresponding follow-up literature,[5–8] have interconnected ferroelectricity, conductivity and demonstrated their coupling. The early predictions by Goltsev et al., according to which the ferromagnetic DWs present in the antiferromagnetic $YMnO_3$ (YMO)[9] contain a ferroelectric DW open the possibility to not only combine conductivity and ferroelectricity but also connect these two with ferromagnetism, which directly implies the possibility to combine spintronics and ferroelectricity. Further theoretical development concluded that if there is a coupling between the order parameters in ferroic materials, chirality could exist in ferroeletric domain walls.[10,11] Also recent reports[12–14] predicted that a net magnetization could be present inside ferroelectric DWs in multiferroics. Regarding crystal symmetry, the space group *R3c* (i.e., that of BFO) allows the magnetization of domain walls.[13] Therefore, it is thus natural to ask whether the specific topology of DWs in ferroelastic BFO would deliver a net magnetic moment and hence, display a sizeable AMR, which would be a relevant spintronics demonstration.

In this work, an AMR of the conductive FE DWs in lithium-doped BFO epitaxial thin films is reported. The electronic transport occurring just through the FE DWs is discriminated from the contribution occuring in the bulk, and the conduction mechanism at the DWs is identified. The extracted contribution of FE DWs to the electronic transport occurs to be responsive to an external magnetic field, with a marked unidirectional anisotropy, accompanied by a visible hysteresis, which is ascribed to the coupling of the FM domain walls to the bulk AFM domains in BFO, similar to that found in FM/AFM structures.[15,16]

To allow the study of the transport properties at the BFO domain walls, we have prepared 100 nm thick high-quality epitaxial $Bi_{0.99}Li_{0.01}FeO_3$ thin films on $SrRuO_3$(80 nm)-covered $SrTiO_3$ (100) single crystal substrates. The good quality of the film and the BFO/SRO interface is illustrated by the transmission electron microscopy (TEM) image of **Figure 1**a (see also SI, section C, Figure S3). Lithium has been used as a dopant to significantly reduce the transport in the bulk of the BFO domains (see SI, section A, Figure S1). Copper top electrodes have been ex-situ deposited to obtain typical metal-ferroelectric-metal planar capacitors of 60 μm lateral size, as sketched in Figure 1b.

The transport mechanism and anisotropic magnetoresistance in this planar geometry was analyzed at different polarization switching states and thus at different effective density of the domain walls. (For the characterization of the pristine DW pattern by PFM, see SI, section B, Figure S2). The first striking result is illustrated in Figure 1c, which shows the AMR of a partially switched BFO capacitor at 5K. The data points follow the dashed lines, which correspond to the fitting of a $\cos^2\theta$ dependence (where θ is the angle between the direction normal to the film and the direction of the magnetic field H), equal to that found in metallic magnets, thus indicating the presence of a net magnetic moment. As we will show later here, we believe

Dr. J. H. Lee, Dr. I. Fina, Dr. Y. H. Kim,
Prof. D. Hesse, Dr. M. Alexe
Max Planck Institute of Microstructure Physics
Weinberg 2
Halle (Saale) D-06120, Germany
E-mail: jihye33@gmail.com;
ignasifinamartinez@gmail.com;
M.Alexe@warwick.ac.uk

Dr. I. Fina, Prof. M. Alexe
Department of Physics
University of Warwick
Coventry CV 4 7AL
United Kingdom

Dr. X. Marti
Department of Condensed Matter Physics
Faculty of Mathematics and Physics
Charles University
12116, Praha 2, Czech Republic

Dr. X. Marti
Centre d'Investigacions en Nanociencia I Nanotechnologia (CIN2)
CSIC-ICN, Bellaterra
08193, Barcelona, Spain

Dr. Y. H. Kim
Korea Research Institute of Standards and Science
Daejeon 305–304, Republic of Korea

DOI: 10.1002/adma.201402558

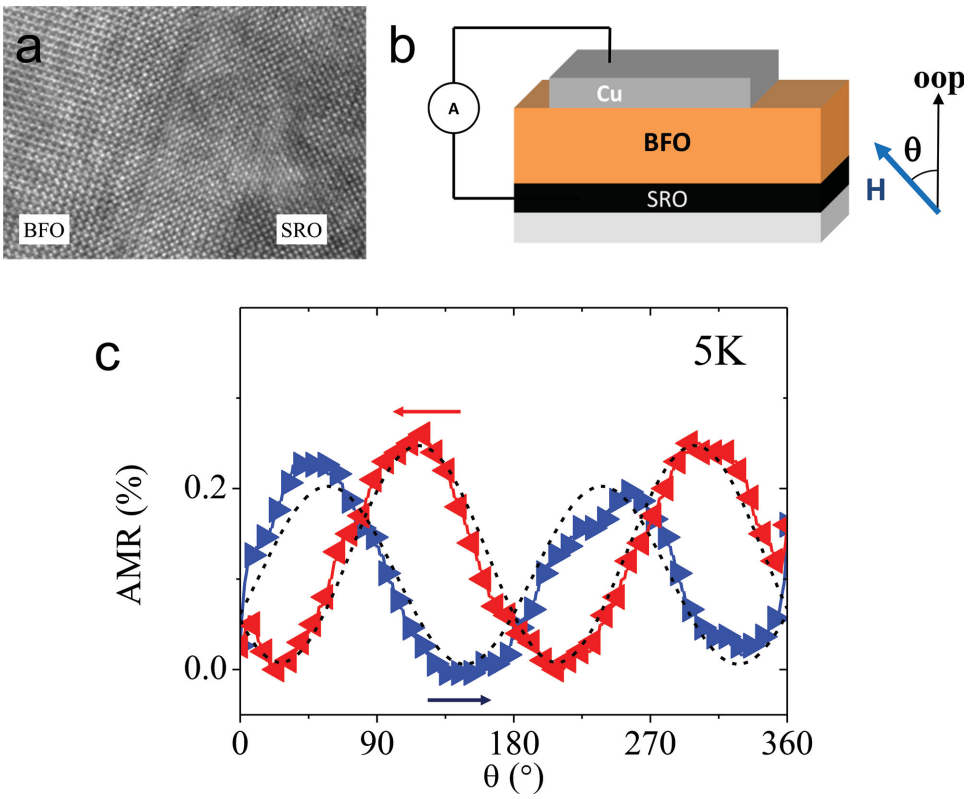

Figure 1. Electric transport influenced by an external magnetic field. a, Cross-sectional high-resolution TEM image of the high-quality BFO/SRO interface. b, BFO MFM capacitor in a plane-parallel configuration. c, Anisotropic magnetoresistance showing strong hysteresis, which implies a net magnetic moment of the DWs.

that this moment is solely coming from the magnetic properties of the DWs in BFO. The visible hysteresis of the AMR reveals the pinning of the net magnetic moment of the DWs to the bulk AFM domains, and disregards a possible contribution of bulk BFO because it can only be understood in presence of two adjacent materials with different magnetic properties.[15,17] These results confirm that not only Goltsev's prediction for YMO is applicable also to our BFO capacitor, revealing the presence of coupled FM and FE DWs. The DWs being ferromagnetic, this implies that the origin of the enhanced conductivity of the DWs may not be a simple electrostatic effect, but could also be a result of the closure of the band gap due to the shift of the band diagram for the spin-up and spin-down states at the DWs. In the next paragraphs, a procedure will be described which allows to distinguish between contributions of the DWs and the bulk to the measured transport properties. Furthermore, the transport mechanism at the DWs will be investigated with a detailed analysis of the AMR-related experiments.

One can easily assume that the effective density of the DWs during switching using voltage pulses with increasing amplitude will also increase until around the coercive field for ferroelectric polarization switching, and then decrease to almost the same value as in the initial state (see SI, section D, Figure S4). A simple geometric model can help to calculate the effective length of the DWs during the switching process (see SI, section E, Figure S5). This calculation is not based on a definite switching mechanism, but rather on a linear relation between the DW length and the switched polarization. Given that three different types of DWs (71°, 109°, and 180° respectively, see SI, section B, Figure S2) are existing in our BFO epitaxial films, it is assumed that all possible ferroelectric/ferroelastic DWs are present in this capacitor geometry. In **Figure 2**a and b, the current measured across the capacitor is plotted in dependence of the voltage amplitude of the pre-applied discrete voltage switching pulses. At room temperature, the effective conductivity of the capacitor switches between two bi-stable states with high and low current, respectively, with an approximately 35% variation in current (Figure 2a), largely reproducing previous results related to the resistive switching of BFO.[18] The effective conductivity shows a completely different behavior at temperatures lower than 100K (Figure 2b), where a clear peak near the coercive field occurs. There is an increase of the conductivity by an order of magnitude when the polarization is half-switched, compared to the situation of a fully switched state, which corresponds to the coercive voltage and coincides with the derivative of the polarization with respect to the switching voltage (Figure 2c at 30K). As it is described in the SI (sections D and E, Figure S4 and S5), the population and effective length of the DWs become maximal exactly at these switching voltages around the coercive voltage. Thus, in this state, one may say that the effective conductivity of the device is merely determined by the DWs, which from the electronic transport point of view act as shunts between the top and bottom electrodes. The estimated length of the domain walls follows the effective conductivity behavior: hence, we estimate the resistivity of the DWs to about 10^6 Ω cm.

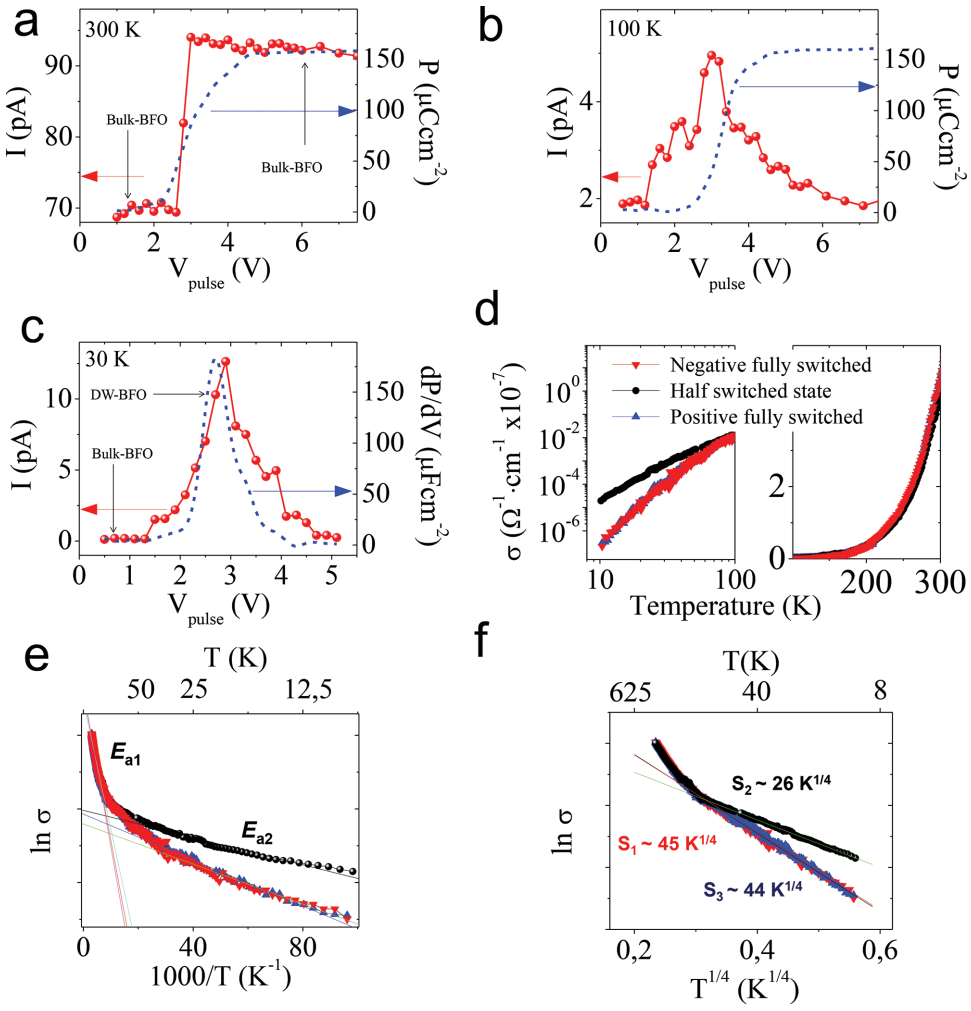

Figure 2. Effective conductivity during partially switching the ferroelectric polarization, and conduction mechanism of the DWs. Steady-state current through the MFM capacitor measured at +0.8 V applied voltage after partial switching of the polarization using a 1 ms triangular pulse with the amplitude shown on the abscissa and measured at a, 300 K and b, 100 K. c, Correlation between the effective conductivity and the polarization switching at 30 K. Polarization measured at each partial switching and the corresponding steady-state current measured with +0.5 V probing voltage. The blue line represents the derivative of the polarization which is proportional to the length of the domain walls (see SI). Note that the current is measured after long time stabilization; respectively it represents the true leakage solely generated by electronic transport. d, Temperature dependence of the effective conductivity of the BFO capacitor in fully negative (red) and positive (blue) state and in partly switched state (black). From below 100 K, the difference of the effective conductivity is distinguishable between the fully switched state and the partly switched state. e, Arrhenius plot of the effective conductivity showing two distinct behavior regimes. f, *ln* σ versus $T^{-1/4}$ plot for all states, respectively. The slope values obtained from the fit are indicated in the figure.

To analyze the origin of the conductivity at the DWs, temperature-dependent transport is investigated. From the very low temperature up to around 100 K, the conductivity shows a significant difference between the fully (negative and positive) and partly switched states (Figure 2d). At 100 K the conduction mechanism of the bulk changes dramatically, inducing a crossover from the DW-controlled to the bulk-controlled conductivity, as it can be inferred in the right panel of Figure 2d. This was confirmed by the Arrhenius-plot fitting in Figure 2e. In the high temperature regime all states show an activation energy of the conduction of about 0.12 eV. In the low temperature regime, the activation energies are very low: 0.8 – 0.9 meV for the fully polarized states (negative and positive) and 0.5 meV for the partly polarized state, as shown in **Table 1**. The difference between the low temperature activation energies indicates a significant qualitative difference between the conduction in the fully and partly switched states, bringing additional evidence to the assumption that in the partly switched state the conduction is governed by the domain walls rather than the bulk. Note also the difference between the high temperature regime, where the two switchable states show similar activation energies (and concomitantly, similar conductivity frameworks), and the low temperature regime, where the difference between the activation energies denote the different nature of the conduction mechanism. In the low temperature regime, the very low values of the activation energy indicate that the conduction mechanism is actually not energy activated, but most probably of a hopping type. If we assume that the conductivity in this low temperature

Table 1. Activation energy (by the Arrhenius-plot fitting), T_0 (the fitting parameter of the VRH equation), and effective density of states $N(E_f)$ values in all three switching cases (the calculated values of VRH equation). $N(E_f)$ was calculated by assuming a hopping range of the order of the unit cell $a \sim 4.3$Å [a)]

	By Arrhenius-plot fitting		*By variable-range-hopping*	
	E_{a1} (High T regime) [eV]	E_{a2} (Low T regime) [meV]	T_0 [K]	N(E_f) [/eV·cm^3]
Fully negative switched state	0.12	0.9	3.75×10^6	8.25×10^{20}
Partially switched state	0.12	0.5	4.56×10^5	6.77×10^{21}
Fully positive switched state	0.12	0.8	4.10×10^6	7.55×10^{20}

[a)]A. Z. Simões, E. C. Aguiar, A. H. M. Gonzalez, J. Andrés, E. Longo, J. A. Varela, *J. Appl. Phys.* **2008**, 104, 104115.

regime is due to a variable-range-hopping (VRH) conduction mechanism, the conductivity should follow the following law:[19]

$$\sigma = \sigma_0 \exp\left[-\left(T_0 / T\right)^{1/4}\right] \quad (1)$$

with

$$T_0 = 21.2 / a^3 k_B N(E_f) \quad (2)$$

where a is a localization length, k_B is Boltzmann's constant, and $N(E_f)$ is the density of states at the Fermi level.[19] Note that in the case of the partially switched state, T_0 has a smaller value than in the fully switched states (see Table 1). The obtained T_0 values are comparable with various other transition-metal oxides.[20–25] Equation (2) shows that the origin of the temperature shift between the two states is the density of states at the Fermi level, which can be estimated. In case of the partially switched state (Table 1), the density of states is one order of magnitude higher than that of the fully switched states. Thus, it can be stated that the density of states at the domain walls 6.27×10^{21} eV^{-1} cm^{-3} is almost an order of magnitude higher than that of the bulk value, 8.25×10^{20} eV^{-1} cm^{-3}.

Having established the route to discriminate between the bulk and DW contributions to the transport, and also the characteristics of the transport mechanism, we resume from here the more detailed description of the found anisotropy in the magnetotransport response. The dependence of the current on the angle θ for the half switched and fully switched BFO film is depicted in **Figure 3**a. The two distinct states are clearly visible, viz. the larger current one (where the DW contribution is larger), and the lower current one (where the bulk contribution has a higher contribution or the domain wall density is very low). On top, it is remarkable that the current dependence on the angle is out of the noise for the half switched state, and any contribution of Lorentz anisotropic magnetoresistance has been disregard because any noticeable magnetoresistance has not been observed (see SI, section F). The dependence for the fully switched state is of the same magnitude, but not with the same trend: The dependence found in the fully switched state is odd with the applied magnetic field angle, resulting from the sum of the few unavoidable DWs (which contribute to the overall signal with a $\cos^2\theta$ shape) and from the larger contribution of the pyroelectric current, which results from small temperature variations.

Now let us turn towards discussing the role of the virtually unavoidable contribution of SRO in the measured AMR, which can show itself a non-zero AMR.[26] Figure 3b shows the AMR measurement for the bottom SRO layer, contacted and measured in the same way as for BFO, but placing the contacts on the sides of the sample (see SI, section F, Figure S6). The collected data reveal that there is no correlation between the measured resistance and the applied magnetic field direction, and that the error bar, defined as statistical deviation from several performed measurements, is smaller than the AMR amplitude measured in the BFO domain walls. This rules out that the BFO-DW AMR stems exclusively from the SRO contribution, although the latter may be present. Further studies on the temperature dependent AMR have been performed without

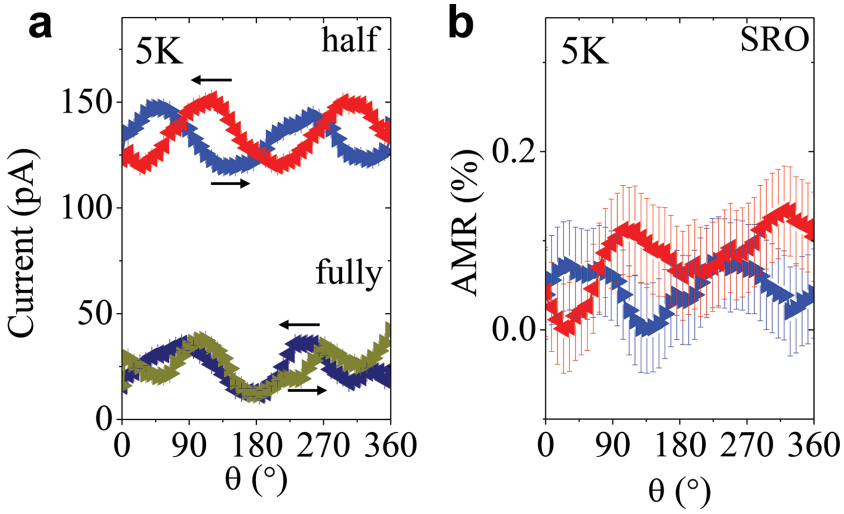

Figure 3. AMR behavior of both states, and SRO contribution. a, Current measured while applying the magnetic field at a certain angle θ with respect to the direction normal to the plane of the films as sketched in Figure 1b for a fully switched (low-current) and half-switched (high current) ferroelectric BFO state at 5 K. Left- and right-triangles denote increasing and decreasing angle. b, AMR measurement for the SRO layer of the same sample. Error bars are averaged for three measurements.

reaching any conclusion, due to the increasing bulk contribution that hinders the genuine AMR from the BFO DWs at temperatures above approx. 20K (see SI, section F, Figure S7).

In summary, macroscopic transport measurements on lithium-doped BFO films show that the effective conduction mechanism is variable range hopping at low temperature, with significant differences of the density of states at the Fermi level between the DWs ($\approx 10^{21}$ eV^{-1} cm^{-3}) and the bulk ($\approx 10^{20}$ eV^{-1} cm^{-3}). The found modulation of the electronic transport across DWs in BFO by an external magnetic field, which shows an AMR at low temperature, allows to make use of the two ferroic orders at nanoscale. The DWs being ferromagnetic implies also that the origin of the enhanced conductivity of the DWs may not be a pure electrostatic effect, but may also result from the closure of the band gap due to the shift of the band diagram for spin-up and spin-down states. Our results open a perspective for using multiferroicity of domain walls for nanoelectronics.

Experimental Section

Fabrication of the BFO Films: $SrRuO_3$ (SRO) bottom electrodes of 80 nm thickness and BFO films of about 100 nm thickness were epitaxially grown on $SrTiO_3$ (100) substrates using pulsed laser deposition (PLD) at 650 °C in 0.15 mbar oxygen pressure with a laser repetition rate of 5 Hz. The KrF excimer laser (wavelength 248 nm) was used at a typical laser fluence of $\approx$ 0.5 J cm^{-2} to ablate a lithium-doped target of nominal composition $Bi_{0.99}Li_{0.01}FeO_3$. After deposition, the films were cooled down to RT at a rate of 15 °C/min with 200 mbar oxygen pressure. SRO was used as a bottom electrode for all electrical measurements in capacitor-like geometry. Pt and Cu top electrodes (60×60 μm^2) were sputtered on the BFO surface using a shadow mask.

Thin Films and Device Characterization: A ferroelectric tester (TF Analyzer 2000, AixaCCt) was used to obtain typical ferroelectric hysteresis curves at 2 kHz and to switch the ferroelectric capacitor devices. Partial switching of polarization has been performed using triangular unipolar pulses of 1 ms duration with different amplitudes. Switching has been performed always from one fully switched state to the respective partially switched state, measuring in the same time the switched polarization. The temperature-dependent current behavior was investigated using a Cryoprobe-station (Lake Shore HTTP4) and a Keithley 6517B electrometer. Current measurements were performed at heating from low to high temperatures with a rate of 1 K/min.

Anisotropic Magnetoresistance: The resistance dependence on the angle θ (the latter defined as $\theta = 0$ when the normal to the film is parallel to the applied magnetic field) was obtained from the current measured using a Keithley 6517B electrometer. The rotating magnetic field was applied using a PPMS (Quantum Design Co.). To obtain an acceptable signal to noise ratio in these measurements several capacitors were measured in parallel (note that this results in larger measured currents).

Supporting Information

Supporting Information is available from the Wiley Online Library or from the author.

Acknowledgements

I.F. acknowledges the Beatriu de Pinós postdoctoral scholarship (2011 BP-A 00220) from the Catalan Agency for Management of University and Research Grants (AGAUR-Generalitat de Catalunya). M.A. acknowledges the Wolfson Merit Research Award of Royal Society. Work in part supported by DFG via SFB 762.

Received: June 10, 2014
Revised: July 22, 2014
Published online: September 23, 2014

[1] J. Ma, J. Hu, Z. Li, C.-W. Nan, *Adv. Mater.* **2011**, *23*, 1062.
[2] W. Thompson, *Proceedings of the Royal Society of London* **1859**, *8*, 546.
[3] J. Valasek, *Phys. Rev.* **1921**, *17*, 475.
[4] J. Seidel, L. W. Martin, Q. He, Q. Zhan, Y.-H. Chu, A. Rother, M. E. Hawkridge, P. Maksymovych, P. Yu, M. Gajek, N. Balke, S. V. Kalinin, S. Gemming, F. Wang, G. Catalan, J. F. Scott, N. A. Spaldin, J. Orenstein, R. Ramesh, *Nat. Mater.* **2009**, *8*, 229
[5] J. Seidel, P. Maksymovych, Y. Batra, A. Katan, S.-Y. Yang, Q. He, A. P. Baddorf, S. V. Kalinin, C.-H. Yang, J.-C. Yang, Y.-H. Chu, E. K. H. Salje, H. Wormeester, M. Salmeron, R. Ramesh, *Phys. Rev. Lett.* **2010**, *105*, 197603
[6] S. Farokhipoor, B. Noheda, *Phys. Rev. Lett.* **2011**, *107*, 127601
[7] P. Maksymovych, J. Seidel, Y. H. Chu, L.-Q. Chen, S. V. Kalinin, R. Ramesh, P. Wu, A. P. Baddorf, *Nano Lett.* **2011**, *11*, 1906
[8] Q. He, C.-H. Yeh, J.-C. Yang, G. Singh-Bhalla, C.-W. Liang, P.-W. Chiu, G. Catalan, L. W. Martin, Y.-H. Chu, J. F. Scott, R. Ramesh, *Phys. Rev. Lett.* **2012**, *108*, 067203
[9] A. V. Goltsev, R. V. Pisarev, Th. Lottermoser, M. Fiebig, *Phys. Rev. Lett.* **2003**, *90*, 177204
[10] D. Lee, R. K. Behera, P. Wu, H. Xu, Y. L. Li, S. B. Sinnott, S. R. Phillpot, L. Q. Chen, V. Gopalan, *Phys. Rev. B* **2009**, *80*, 060102
[11] P. Marton, I. Rychetsky, J. Hlinka, *Phys. Rev. B* **2010**, *81*, 144125
[12] J. Privratska, V. Janovec, *Ferroelectrics* **1997**, *204*, 321
[13] J. Privratska, V. Janovec, *Ferroelectrics* **1999**, *222*, 23
[14] J. Privrastka, *Ferroelectrics* **2007**, *353*, 116
[15] J. Nogués, I. K. Schuller, *J. Mag. Mag. Mater.* **1999**, *192*, 203
[16] T. Gredig, I. N. Krivorotov, E. D. Dahlberg, *Phys. Rev. B* **2006**, *74*, 094431
[17] J. Nogués, J. Sort, V. Langlais, V. Skumryev, S. Suriñach, J. S. Muñoz, M. D. Baró, *Phys. Rep.* **2005**, *422*, 65
[18] A. Q. Jiang, C. Wang, K. J. Jin, X. B. Liu, J. F. Scott, C. S. Hwang, T. A. Tang, H. B. Lu, G. Z. Yang, *Adv. Mater.* **2011**, *23*, 1277
[19] N. F. Mott, E. A. Davis, *Electronic Processes in Non-crystalline materials*, Clarendom Press, Oxford, **1971**, Chap 2
[20] M. Jenderka, J. Barzola-Quiquia, Z. Zhang, H. Frenzel, M. Grundmann, M. Lorenz, *Phys. Rev. B* **2013**, *88*, 045111
[21] M. A. Kastner, R. J. Birgeneau, C. Y. Chen, Y. M. Chiang, D. R. Gabbe, H. P. Jenssen, T. Junk, C. J. Peters, P. J. Picone, T. Thio, T. R. Thurston, H. L. Tuller, *Phys. Rev. B* **1988**, *37*, 111
[22] M. Bremholm, S. Dutton, P. Stephens, R. Cava, *R. J. Solid State Chem.* **2011**, *184*, 601
[23] R. H. Colman, A. C. McLaughlin, *Phys. Rev. B* **2012**, *85*, 144419
[24] A. Yildiz, S. Lisesivdin, M. Kasap, D. Mardare, *J. Non-Cryst. Solids* **2008**, *354*, 4944
[25] M. Lorenz, H. von Wenckstern, M. Grundmann, *Adv. Mater.* **2011**, *23*, 5383
[26] L. Klein, J. S. Dodge, C. H. Ahn, G. J. Snyder, T. H. Geballe, M. R. Beasley, A. Kapitulnik, *Phys. Rev. Lett.* **1996**, *77*, 2774